ELSEVIER

Journal of Structural Geology 27 (2005) 1426–1444

JOURNAL OF STRUCTURAL GEOLOGY

www.elsevier.com/locate/jsg

Emplacement-related fabric and multiple sheets in the Maiden Creek sill, Henry Mountains, Utah, USA

Eric Horsman[a,*], Basil Tikoff[a], Sven Morgan[b]

[a]*Department of Geology and Geophysics, University of Wisconsin, Madison, WI 53706, USA*
[b]*Department of Geology, Central Michigan University, Mt Pleasant, MI 48859, USA*

Received 10 June 2004; received in revised form 21 February 2005; accepted 11 March 2005
Available online 26 July 2005

Abstract

The Maiden Creek sill is a small intrusion ($\sim$1 km^2 in map view) that is part of the Tertiary igneous complex of the Henry Mountains in southern Utah. Field relationships indicate that (1) this sill has a complex map view geometry, consisting of an elliptical main body from which radiate several finger-like lobes; (2) the intrusion is composed of two igneous sheets, presumably representing distinct magma pulses; and (3) the current exposure of the intrusion corresponds closely to the original intrusive geometry. These relationships allow us to examine in detail the relationships between fabric development, intrusive geometry, and emplacement processes in this intrusion.

This sill was emplaced into the flat-lying sediments of the Colorado Plateau during a time of tectonic quiescence. Fabrics within the intrusion can therefore be interpreted in terms of igneous emplacement processes. Fabric data are derived from field measurements, image analysis, X-ray computed tomography, and anisotropy of magnetic susceptibility. In the center of each sheet, magmatic fabrics are subhorizontal and poorly defined. In the outermost 5–15 cm of each sheet, solid-state fabrics are developed sub-parallel to the contact. The two distinct intrusive sheets have similar composition, thickness, and areal extent. We infer that emplacement of the first sheet established the initial map view geometry of the intrusion and the second sheet closely followed the contact between that first sheet and the host rock. The example of the Maiden Creek sill demonstrates that sheeted emplacement can be an important process even in the early stages of construction of small intrusions, in addition to other larger intrusions studied elsewhere.

Keywords: Pluton emplacement; Sheet intrusion; Sill; Fabric; Henry Mountains

1. Introduction

Making a direct correlation between fabrics in igneous rocks and magmatic flow is problematic for several reasons. For example, fabric may result from multiple overprinting events (e.g. emplacement, syn-emplacement deformation, post-emplacement deformation) and it reflects finite strain, produced by progressive magmatic flow, rather than flow directions. Furthermore, because the exposure of most igneous bodies (in particular contacts with host rock) is limited, the boundary conditions for these deformations are rarely known. These complicating factors and others often make it difficult to unambiguously interpret igneous fabrics (Hutton, 1988; Paterson et al., 1998).

The intrusions of the Henry Mountains of south-central Utah provide a field setting that allows many of the above difficulties to be overcome. The igneous bodies intrude the well-documented flat-lying stratigraphy of the Colorado Plateau, so displacement of the wall rocks resulting from igneous intrusion can be well constrained (e.g. Hunt, 1953; Pollard and Johnson, 1973; Jackson and Pollard, 1988). The intrusions are mid-Tertiary in age (Nelson et al., 1992) and therefore postdate any orogenic activity in the area. Consequently, fabric within the intrusion records primarily finite strain produced by magmatic flow during emplacement and lacks a significant concurrent or subsequent tectonic overprint.

This study is focused on the Maiden Creek intrusion, a small ($\sim$1 km^2 outcrop area) sill-like body in the Henry Mountains. This particular intrusion was studied because of its small size and exceptional exposure, which allows an

* Corresponding author. Fax: +1 608 262 0693.
E-mail address: eric@geology.wisc.edu (E. Horsman).

0191-8141/$ - see front matter © 2005 Elsevier Ltd. All rights reserved.
doi:10.1016/j.jsg.2005.03.003

accurate determination of its original three-dimensional geometry. As a result, we can examine in detail the effects of three-dimensional intrusion geometry and igneous emplacement mechanisms on fabric development.

In order to document fabric within the intrusion, we used a variety of techniques, including field mapping, anisotropy of magnetic susceptibility, and shape preferred orientation analysis from both image analysis and X-ray computed tomography. The Maiden Creek intrusion's simple emplacement history, well constrained three-dimensional geometry and small size make it an ideal body on which to examine the relationships between magmatic flow during emplacement and the development of fabric.

2. Geological setting

2.1. The Henry Mountains

The Henry Mountains of south-central Utah are a large Tertiary igneous complex on the Colorado Plateau (Fig. 1a). The range is composed of five distinct igneous centers that were emplaced into the shallowly west-dipping (1–2°) limb of an asymmetric syncline (Fig. 1b). Each igneous center is composed of a large central intrusion from which numerous smaller intrusions radiate (Gilbert, 1877; Hunt, 1953; Jackson and Pollard, 1988).

The igneous rock of the Henry Mountains is a homogeneous plagioclase–hornblende porphyry in which phenocrysts of feldspar and amphibole lie in a very fine-grained gray matrix (Hunt, 1953; Engel, 1959; Nelson et al., 1992). Feldspar phenocrysts make up 30–35% of the rock by volume and are generally euhedral laths 0.2–1 cm in diameter. Amphibole phenocrysts make up 5–15% of the rock by volume and are euhedral needles 0.1–0.5 cm in length. Other phenocrysts include euhedral to subhedral oxide grains, which generally have a maximum diameter of 0.2 mm and make up less than 2% of the porphyry by volume, and apatite and sphene, both of which are generally euhedral and less than 1% by volume. The very fine-grained matrix generally makes up 50% or more of the rock and is composed of microcrystalline feldspar, amphibole, and oxides.

2.2. The Mt Hillers intrusive center and the Maiden Creek sill

Mt Hillers (Fig. 1b) is the best exposed of the five Henry

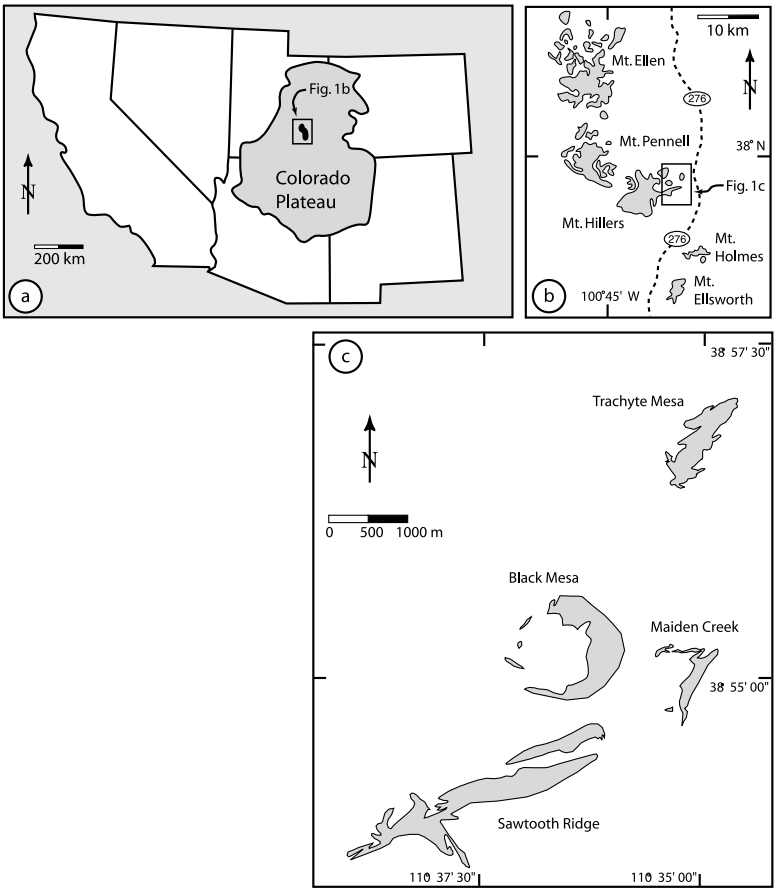

Fig. 1. Location maps. (a) The Colorado Plateau region in the western US Cordillera with the location of the Henry Mountains indicated. (b) The five intrusive centers of the Henry Mountains with the location of (c) indicated. (c) Intrusions on the eastern edge of the Mt Hillers igneous center (intrusions shaded in gray). The surrounding sedimentary rocks dip very shallowly to the west. Parts (a) and (b) modified from Nelson et al. (1992).

Mountains intrusive centers. Cumulatively, the intrusions of Mt Hillers have vertically displaced the surrounding sediments ~2.5 km, with the result that the mountain presently forms a dome with a diameter of ~15 km (Hunt, 1953; Jackson and Pollard, 1988). Several steep, narrow canyons cut into Mt Hillers and expose cross-sections through numerous intrusions radiating away from the center of the dome. This exposure allows examination of both the intrusions themselves, which vary widely in size and geometry, and the complex feeding relationships between the numerous intrusions.

Several small intrusions outcrop on the easternmost flank of Mt Hillers at a distance of 8–10 km from the center of the mountain (Fig. 1c). These bodies are well enough exposed for Hunt (1953) and Johnson and Pollard (1973) to characterize their three-dimensional geometries, including an elongate laccolith (Sawtooth Ridge), a bysmalith or punched laccolith (Black Mesa; see Habert and de Saint Blanquat, 2004), a transitional sill-laccolith (Trachyte Mesa), and the Maiden Creek sill. The Maiden Creek intrusion is one of the most distal exposed portions of the Mt Hillers intrusive center and is intruded entirely within the Entrada sandstone of the Jurassic San Rafael Group (Gilbert, 1877; Hunt, 1953; Johnson and Pollard, 1973).

3. The Maiden Creek sill

3.1. Field observations

3.1.1. Lateral contacts

Lateral contacts of the Maiden Creek intrusion with surrounding sediments are exposed in several locations (Figs. 2 and 3). In cross-section, a distinctive bulbous geometry of the igneous rock is present at all of these exposed lateral contacts between the intrusion and the surrounding sediments (Fig. 4a). Similar bulbous lateral terminations have been observed at the margin of the nearby Trachyte Mesa intrusion (Hunt, 1953; fig. 6 in Johnson and Pollard, 1973; Pollard et al., 1975; Morgan et al., in review). At several locations the sediments adjacent to the lateral contact of the sill have recently been eroded, leaving only the bulbous lateral terminations of the intrusion itself (cf. Fig. 4a and b). Where these contacts are preserved, sediments appear almost entirely unmetamorphosed except for rare local precipitation of mm-scale concretion-like spheres that appear to be related to late fluid migration.

The abundance of the lateral contacts of the sill with wall rock suggests that the current map pattern of the sill corresponds very closely to the original geometry of the intrusion and is not the result of erosion of a larger body with a simpler map view shape. This original intrusive geometry can be divided into two distinct parts, (1) the main body of the intrusion, and (2) the finger-like lobes that project out from the main body of the intrusion.

3.1.2. Main body

In map view, the main body of the Maiden Creek intrusion has a slightly elliptical shape, a geometry that is commonly observed in laccolithic intrusions (Corry, 1988). In cross-section (Fig. 3e), the main body has a tabular shape and is concordant with bedding in the surrounding Entrada sandstone. The lateral margin of the main body of the Maiden Creek intrusion is well exposed along a cliff that outlines the eastern edge of the exposure (Fig. 4b). Along this cliff the intrusion is 30–40 m thick and has a well-exposed, concordant upper contact with the overlying Entrada sandstone. Along this cliff the intrusion has two vertically stacked bulbous lateral terminations. The lower contact of the main body with the underlying Entrada is not clearly exposed in this area. However, field relations and the simple, well-known cross-sectional geometry elsewhere (Fig. 4c) suggests that the lower contact of the main body is concordant with bedding in the underlying subhorizontal sediments.

3.1.3. Finger-like lobes

In map view, three large finger-like lobes ('fingers') of the Maiden Creek intrusion are clearly distinguishable (Fig. 2) and strong evidence exists for a fourth lobe in the southwest part of the intrusion. Clear top, bottom and lateral contacts with surrounding sedimentary rocks allow the accurate determination of the three-dimensional geometry of each of these finger-like lobes. These contacts demonstrate that the finger-like lobes project out from the main body of the intrusion and are not merely erosional remnants of a main body that was once larger and has been dissected by streams. No clear textural boundary exists between the main body of the intrusion and the finger-like lobes.

Each finger is 200–400 m long and is distinctly elongate with respect to both its cross-sectional thickness and map view width (Fig. 3a and b). In longitudinal cross-section (Fig. 3a and d) each finger thins progressively away from the main body. The finger shown in Fig. 4a thins from ~30 m thick near the main body to ~7 m thick over a distance of ~400 m. This thinning occurs as the base of the intrusion cuts up gradually through the sedimentary section while the top of the intrusion resides at a consistent bedding-parallel stratigraphic level.

As shown in Fig. 3d, an ephemeral stream has cut through the entire thickness of the intrusion in the south-eastern finger (~35 m thick), exposing a complete E–W cross-section. The bottom contact at this location is planar and concordant with bedding in the underlying Entrada sandstone, which is locally composed of shale (Fig. 4c).

3.1.4. Igneous–igneous contacts and intercalated sediments

Contacts between separate sheets of igneous material are rarely distinguishable (e.g. Fig. 4e). Where observed, these igneous–igneous contacts are defined by a thin zone of intense solid-state deformation (~5 cm thick), on either side of which is a zone of magmatic fabric that decreases in strength away from the contact. Where present, these

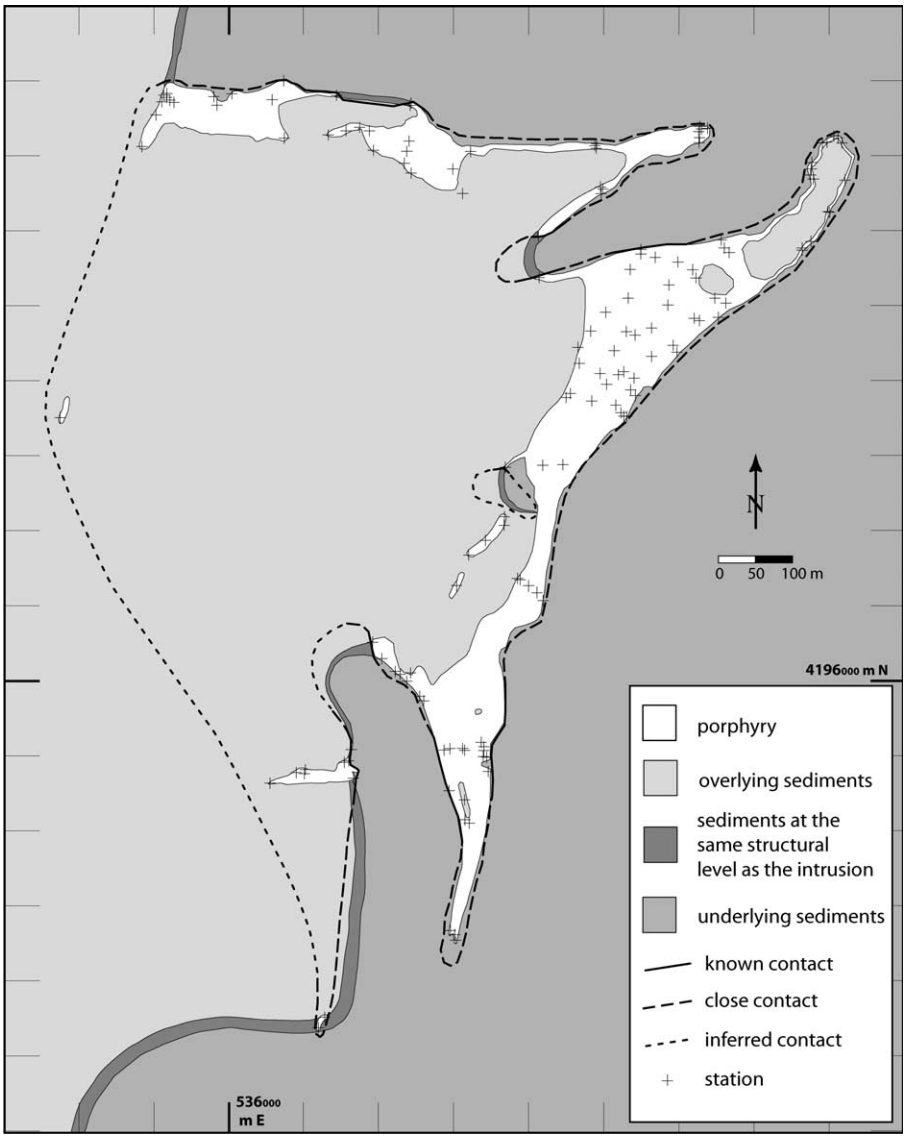

Fig. 2. Geological map of the Maiden Creek sill. The intrusion was emplaced parallel to subhorizontal bedding entirely within the Jurassic Entrada sandstone. Shades of gray on this figure indicate the structural level of exposed sediments with respect to the sill. UTM grid spacing is 100 m.

contacts are generally subhorizontal, parallel to the top and bottom contacts of the intrusion with the country rock exposed elsewhere.

Tabular blocks of sedimentary rock occur within the intrusion at several locations. These intercalated bodies of sediment range in thickness from ~5 cm to ~5 m or more, and consist exclusively of the Entrada sandstone. The largest blocks of intercalated sandstone consistently appear half way up between the floor and roof of the intrusion (Fig. 3a). These blocks sometimes appear to have been trapped between different sheets of igneous material and in those cases sometimes correspond spatially with igneous–igneous contacts.

3.2. Multiple intrusive sheets

Our field observations suggest that the Maiden Creek sill was emplaced as a series of sequentially intruded, relatively thin igneous sheets rather than as a single, relatively voluminous pulse of magma. Bulbous terminations occur at the lateral margins of each igneous sheet and are continuous along these margins (Fig. 4b). Cross-sections through the intrusion (Fig. 3) show that the lateral margins of the intrusion are everywhere composed of two bulbous terminations. Along the margins these terminations maintain a constant stratigraphic level and radius of curvature. This lateral continuity of each bulbous termination suggests it was created by a single igneous sheet.

Igneous–igneous contacts and intercalated sediments independently verify this hypothesis. Igneous–igneous contacts may result from either the sequential emplacement of separate sheets or internal deformation of a single sheet during emplacement. As the igneous–igneous contacts on the Maiden Creek sill are sometimes associated with large

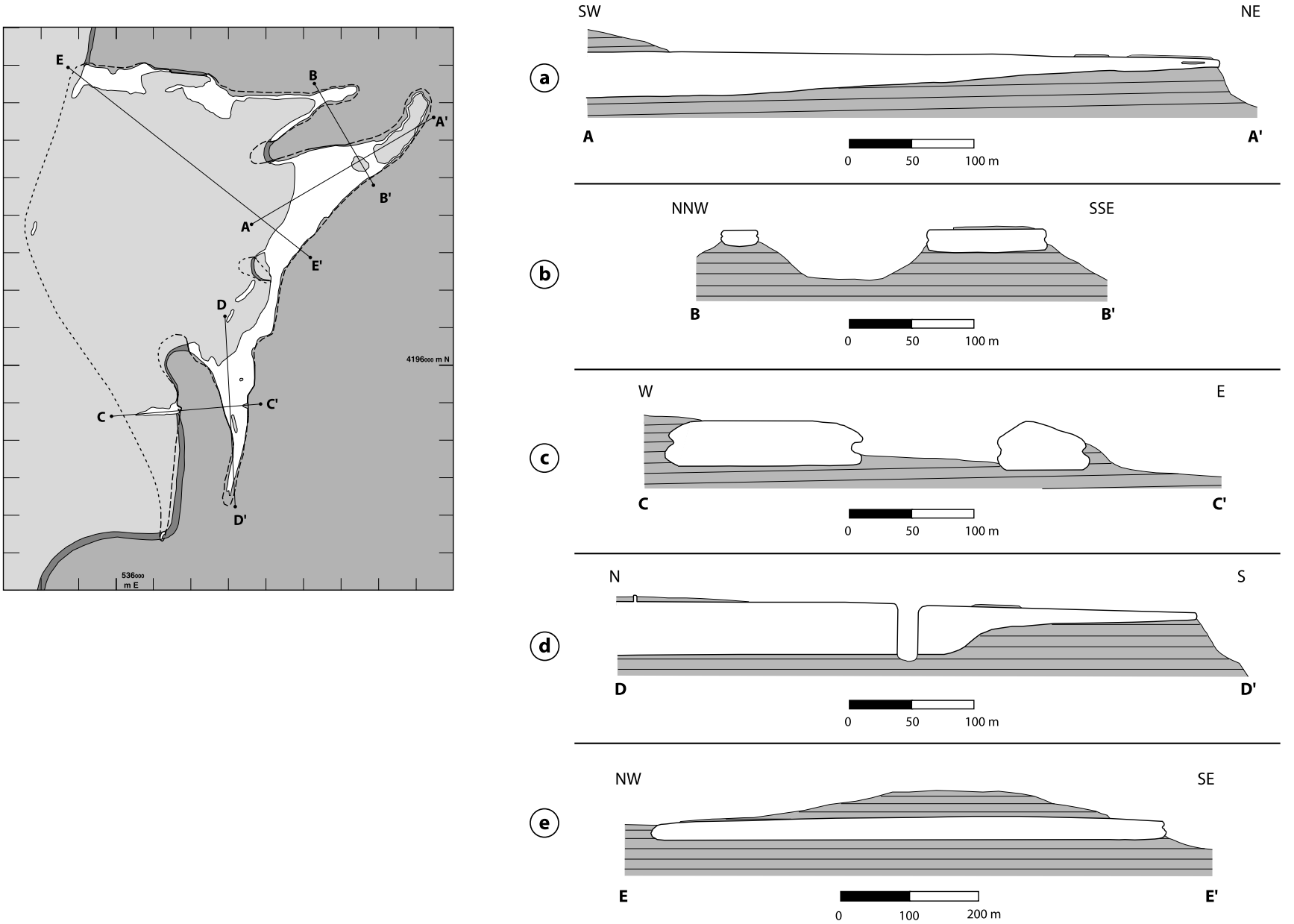

Fig. 3. Cross-sections through the Maiden Creek sill—no vertical exaggeration. Cross-section locations are given on the inset map of the intrusion. In general, the roof of the intrusion is subhorizontal and thinning of the sill results from the upward slope of the bottom of the intrusion.

blocks of intercalated sediment, we consider the contacts to be evidence for separate sheets.

4. Fabric determination

Several techniques were used to characterize fabric in the Maiden Creek sill, including (1) field fabrics, as defined by the alignment of elongate phenocrysts; (2) the shape-preferred orientation of particular minerals, determined using both image analysis and X-ray computed tomography; and (3) the anisotropy of magnetic susceptibility, which records primarily the orientation of ferromagnetic grains within the porphyry. Using multiple fabric determination techniques allows us not only to characterize the fabric within the Maiden Creek intrusion but also to compare the results from the different methods.

4.1. Field measurements

Field observations were made at 130 stations within the Maiden Creek intrusion (Fig. 2). Oriented samples of the porphyry were taken from 97 of these stations for laboratory fabric analysis. We note that, because of the close correspondence between the exposure of the Maiden Creek intrusion and the original geometry of the body, there is a sampling bias toward stations located near the contacts of the intrusion with surrounding wall rock. This problem was somewhat alleviated by sampling natural cross-sections through the intrusion where possible.

4.1.1. Results

Both magmatic and solid-state fabrics are observed within the Maiden Creek intrusion. Magmatic deformation both in the field and in thin section is characterized by the shape-preferred orientation of undeformed feldspar and amphibole phenocrysts. Away from intrusion contacts, fabrics are essentially all magmatic and the strength of this magmatic fabric decreases progressively with increasing distance from the margin. In locations where field measurements are possible, both foliation and lineation are generally subhorizontal. In map view, field-measured magmatic lineations in the main body of the intrusion have a radial pattern while magmatic lineation in each finger is generally subparallel to the long axis of the finger.

Solid-state deformation is identified in the field by a mineral stretching fabric defined primarily by deformation of feldspar and amphibole phenocrysts (Fig. 4f). Thin section analysis indicates that solid-state deformation occurs by extensive fracturing of feldspar and amphibole phenocrysts. Solid-state fabric development is limited to the outermost 5–15 cm of the intrusion. Away from the extreme margins of the intrusion solid-state deformation is confined to rare mm-scale zones that appear to be associated with post-emplacement sub-solidus fracturing of the intrusion (e.g. Bouchez et al., 1992), presumably due to cooling-related contraction of the body.

On the exposed top contacts of the intrusion with recently eroded overlying sediments, a lineation defined by deformed feldspar phenocrysts is very consistent ($\pm 5°$) at the scale of a square meter (Fig. 4f); and is nearly as consistent ($\pm 10°$) over a few square meters. Lineation orientations become more complex near bulbous lateral contacts, a feature considered further in Section 5.

Sense of shear can be determined from obliquity of solid-state fabric with respect to contacts between the intrusion and wall rock (Blanchard et al., 1979; Ramsay, 1980; Wada, 1992; Correa-Gomes et al., 2001). Where sense of shear is measurable, it shows a consistent map view pattern that consistently suggests magma flowed radially away from the center of the main body and out into the fingers (Fig. 5). In cross-section, this pattern suggests that the middle of each sheet flowed outward with respect to both the top and the bottom.

4.2. SPO by image analysis

Documenting the shape-preferred orientation (SPO) of minerals in igneous rocks is a useful, objective technique for quantifying rock fabric (Benn and Allard, 1989; Launeau et al., 1990; Launeau and Cruden, 1998). Spatial analysis of digital images (image analysis) is one commonly used method of SPO determination.

4.2.1. Application

For this study, three oriented mutually orthogonal large (5×7 cm) thin sections were made from each of four oriented hand samples collected from the Maiden Creek intrusion (Fig. 5). Regions of solid-state deformation were avoided so that the magmatic fabric (Fig. 6a) could be isolated. A series of digital photomicrographs of each thin section was taken in plane-polarized light. Each series of photomicrographs was combined into a mosaic for each thin section. These composite images were digitally filtered to accentuate the boundaries of the mineral grains to be analyzed (amphibole, oxide and feldspar).

Following image filtering, a separate traced digital image of each mineral phase was created for each thin section. Thus, three mutually orthogonal images were created for each phase from each of the four hand samples. The two-dimensional SPO of each image was then calculated with SPO2001, a computer program written by P. Launeau and P. Robin that uses the intercept method (Launeau and Robin, 1996) to calculate the SPO of a population of objects on a digital image. The three SPO ellipses for each phase were then combined into a three-dimensional SPO ellipsoid with Ellipsoid2001, a computer program also written by Launeau and Robin (2001). This mathematical methodology is described by Robin (2002). Separate SPO ellipsoids for oxide, amphibole and feldspar were calculated for each of the four hand samples.

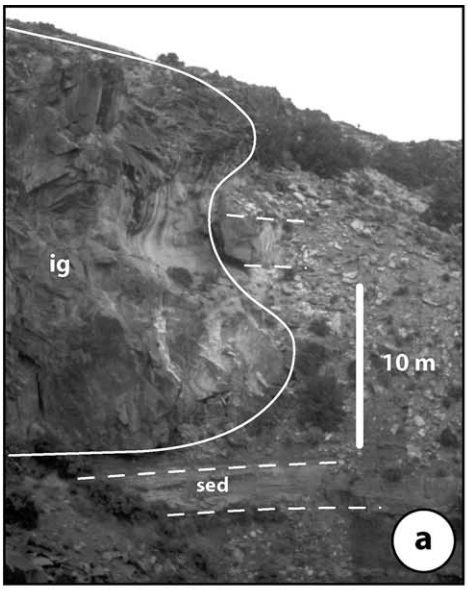
ig
10 m
sed
a

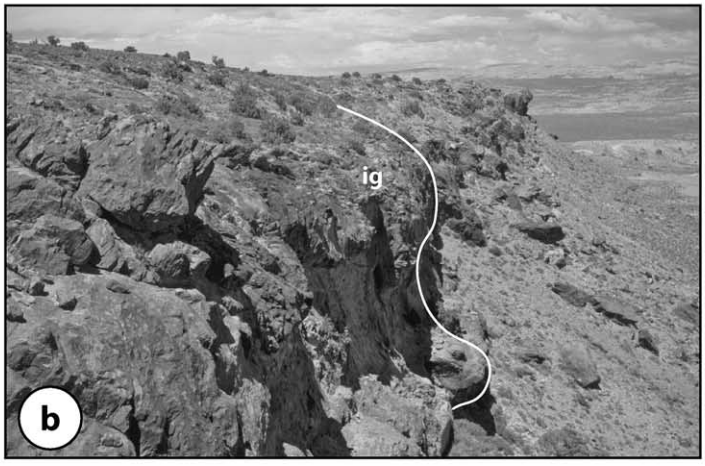
ig
b


ig
3 m
sed
c

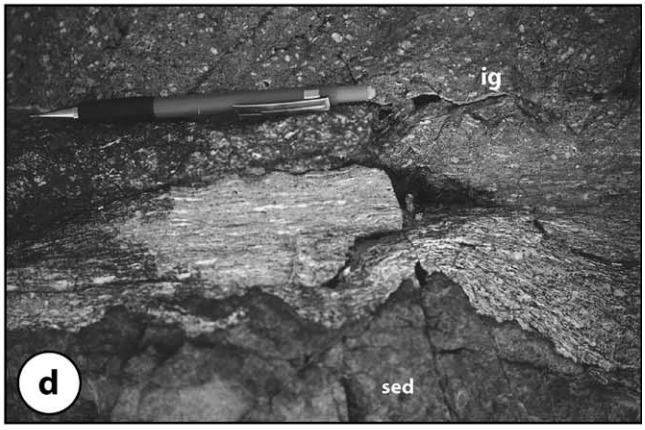
ig
d
sed

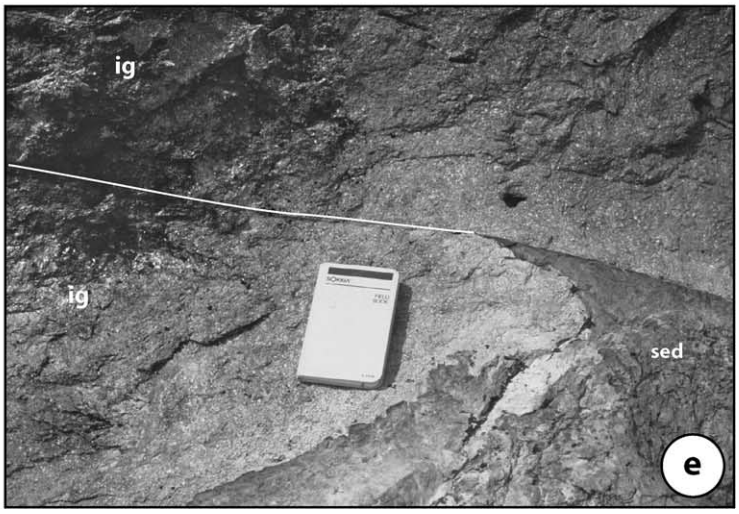
ig
ig
sed
e


f

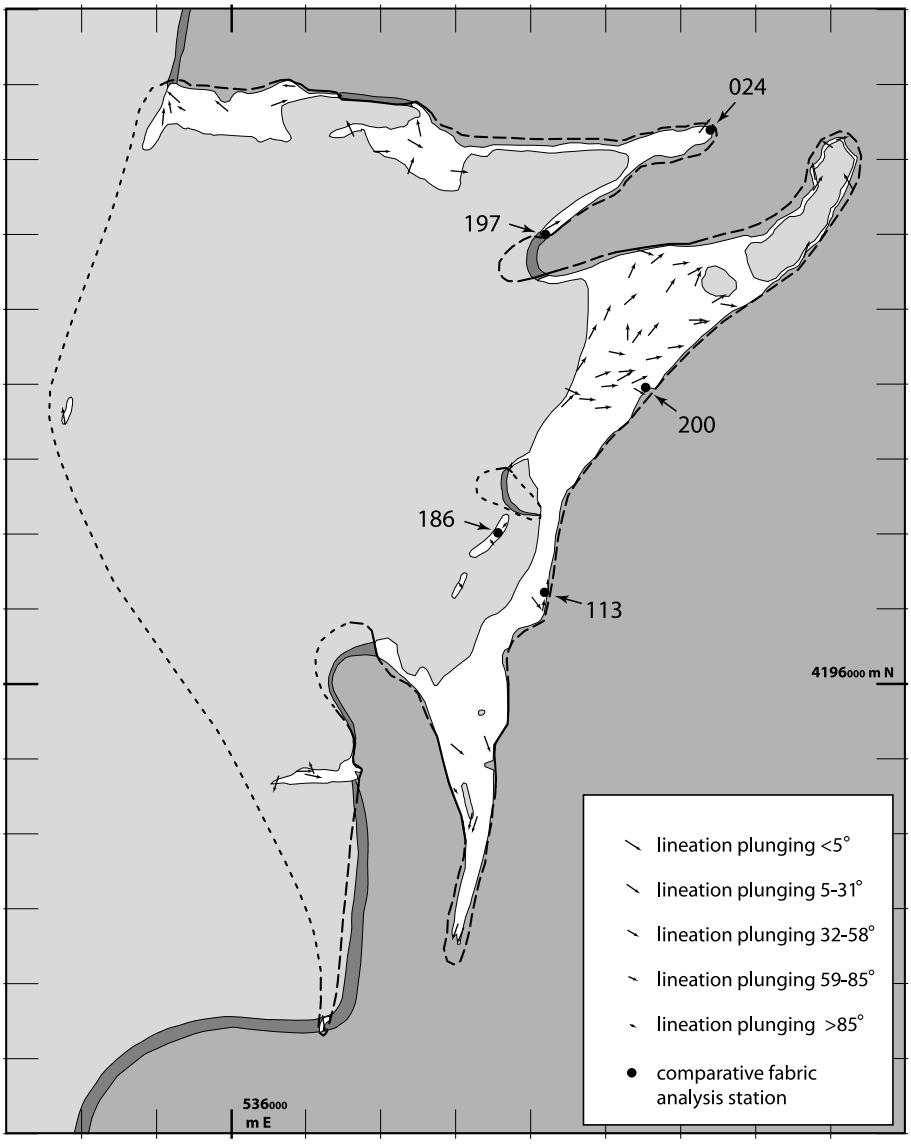

Fig. 5. Field lineation measurements plotted on the geological map of the Maiden Creek sill. See Fig. 2 for map unit legend. Also plotted are the locations of the five stations from which samples were collected for comparative fabric analysis.

One drawback of the image analysis technique as used in this study is its inability to take into account very fine grains. This problem arises from the large thin sections used, which necessitated using low magnification during acquisition of the photomicrographs. This low magnification was sufficient to distinguish phenocrysts of feldspar and amphibole, but insufficient to resolve many of the very small oxide grains. Only grains 0.5 mm and larger in diameter survived the image processing procedures. The largest oxide grains are ~0.5 mm in diameter and the majority are smaller than 0.2 mm. These small oxide grains are ubiquitous within the groundmass of the porphyry. Consequently, the majority of the oxide grains were ignored during the image processing. Those relatively large oxide grains that were resolved with image analysis tend to yield poor SPO results because of the sub-equidimensional shape of the crystals. However, thin

Fig. 4. Field photos of the Maiden Creek sill. Regions of igneous (ig) and sedimentary (sed) rock are labeled. (a) Two bulbous lateral terminations (outlined in white) stacked one atop the other. The adjacent sandstone is still in place. (b) Looking NE along the exposed margin of the main body, stacked bulbous lateral terminations are now devoid of host rock. The bulbous terminations visible in the foreground (outlined in white) extend the entire length of the intrusion as seen in this photo. The intrusion is ~30 m thick in the foreground. (c) The bottom contact of the sill with underlying sediments. The contact is concordant with bedding in the underlying shale. The photo is ~10 m from top to bottom. (d) Solid-state fabric in the sill, adjacent to the wall rock, grades over a short distance into magmatic fabric. (e) Igneous–igneous contact highlighted in white. (f) Solid-state lineation on top of the intrusion.

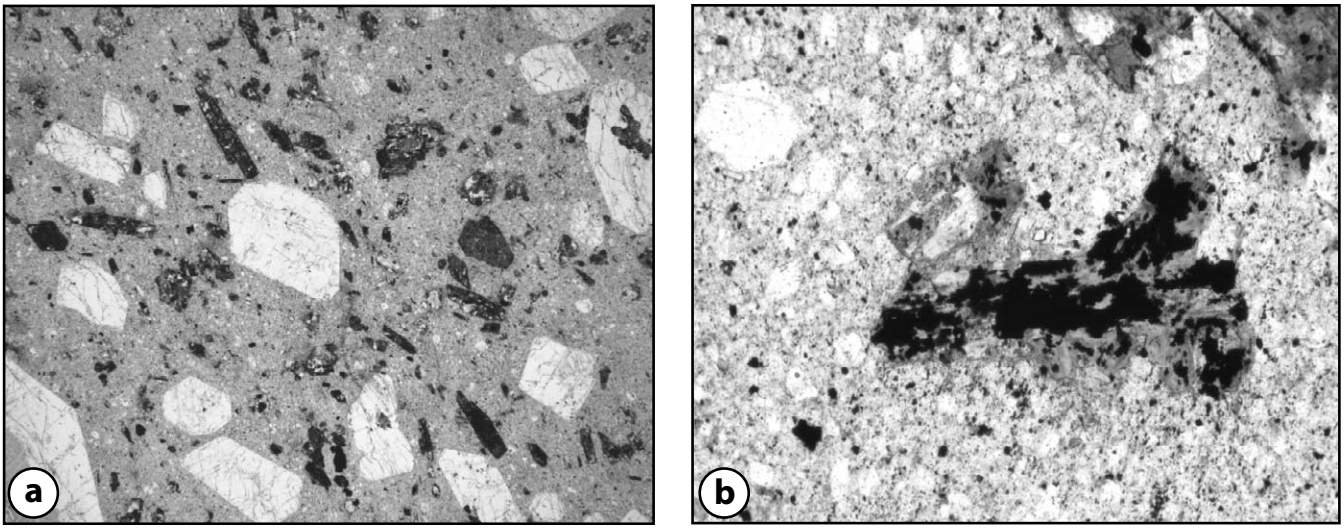

Fig. 6. Photomicrographs of the Maiden Creek sill porphyry. (a) Magmatic fabric defined by the shape-preferred orientation of amphibole and feldspar phenocrysts. The photomicrograph is ~1.5 cm across and was taken in plane-polarized light. (b) Oxides (principally magnetite) have locally replaced amphibole due to deuteric alteration. Secondary oxide shape-preferred orientation is controlled by primary amphibole shape-preferred orientation. The photomicrograph is ~0.5 cm across and was taken in plane-polarized light.

section analysis suggests that many of these large grains were produced during post-emplacement alteration of the porphyry because they replace amphibole and their SPO is controlled by the orientation of primary amphibole (Fig. 6b).

4.2.2. Results

The results of the image analysis are plotted on equal angle, lower hemisphere stereographic projections on Fig. 7. In general, the orientation results for all three separate phases (i.e. feldspar, amphibole and oxide) agree to $\pm 20°$ of one another. Because of the limited number of samples, we principally used results obtained through image analysis for comparison with results of other fabric analysis techniques. Interpretation and discussion of results is given in Section 4.5.

4.3. SPO by X-ray computed tomography

X-ray computed tomography (CT) is a non-destructive method of determining the size, orientation, and distribution of different density materials within a solid body. The results allow the bulk distribution and orientation of the different density materials (e.g. different mineral phases) to be quantified. A brief overview of the theory and process of the analysis techniques is presented in Appendix A, summarized from Herman (1980), Wellington and Vinegar (1987), Flannery et al. (1987) and Denison et al. (1997).

4.3.1. Results

Five cylindrical specimens of the Maiden Creek intrusion porphyry were analyzed at the High Resolution X-ray Computed Tomography Facility at the University of Texas, Austin. Each specimen measured approximately 25 mm in diameter and 22 mm in length. Specimens with solid-state deformation were avoided. In each specimen three distinct narrow density ranges were generally distinguishable from the matrix of the porphyry. These density ranges correspond to oxides (relatively high density), amphibole (relatively low density), and feldspar. Feldspar was often difficult to distinguish from the matrix, so results for this phase are less reliable than for the oxide and amphibole phases. The orientations of the SPO ellipsoid for oxides, amphibole and feldspar in the five samples analyzed are plotted on Fig. 7. Interpretation and discussion of CT results relative to the other fabric determination techniques is given in Section 4.5.

4.4. Anisotropy of magnetic susceptibility

The low-field anisotropy of magnetic susceptibility (AMS) of oriented samples was measured to objectively quantify rock fabric within the Maiden Creek intrusion (e.g. Hrouda, 1982; Borradaile, 1988; Tarling and Hrouda, 1993; Borradaile and Henry, 1997; Bouchez, 1997). The AMS method is particularly useful in igneous rocks with weak fabrics, where measurement of field fabric may be difficult. However, care must be taken to interpret AMS results in light of such factors as the magnetic minerals controlling the signal (e.g. Rochette et al., 1992) and the possible presence of composite fabrics (e.g. Tomezzoli et al., 2003). AMS results are described with an ellipsoid whose long, intermediate and short principal axes are, respectively, K_1, K_2, and K_3. From these axes several additional parameters are calculated: (1) K_b, the bulk susceptibility, is a measure of the abundance and variety of magnetic grains. This parameter is defined as $K_b = (K_1 + K_2 + K_3)/3$. (2) T, the mean shape factor, quantifies the shape of the AMS ellipsoid

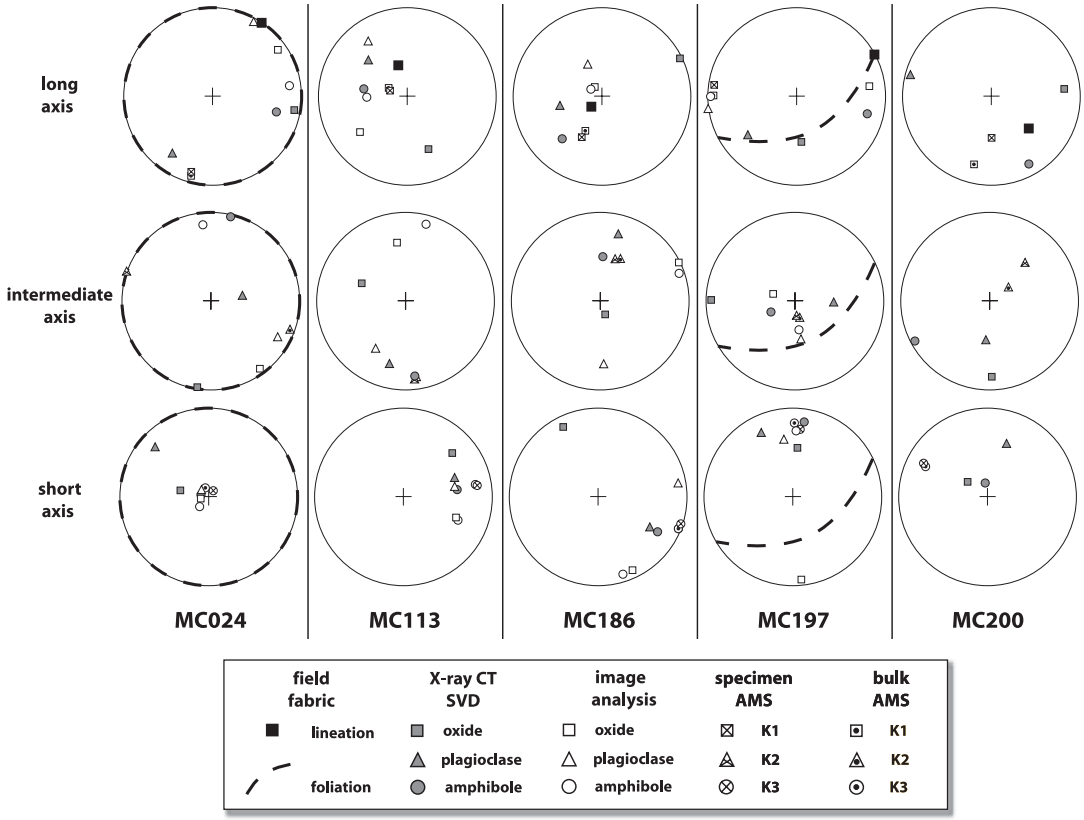

Fig. 7. Comparison of orientation results from the fabric analysis techniques. All results are plotted on equal-angle lower hemisphere stereographic projections. For each of the five stations, long, intermediate, and short axes of the fabric ellipsoids from the various techniques are plotted on separate diagrams. Note that image analysis was not performed on sample MC200. Field fabric is shown for station where it was measurable.

with respect to a sphere ($T=0$), where an infinitely prolate ellipsoid has $T=-1$ and an infinitely oblate ellipsoid has $T=1$. This parameter is defined as $T=[2\ln(K_2/K_3)/\ln(K_1/K_3)]-1$. (3) P', the mean calculated degree of anisotropy, quantifies the intensity of the AMS ellipsoid and hence fabric intensity. This parameter is defined as $P'=\exp(2[(\eta_1-\eta_b)^2+(\eta_2-\eta_b)^2+(\eta_3-\eta_b)^2]^{1/2})$ where $\eta_i=\ln K_i$ and $\eta_b=\ln(\eta_1\times\eta_2\times\eta_3)^{1/3}$.

4.4.1. Application

The AMS was measured on oriented samples taken from 75 stations on the Maiden Creek intrusion. Care was taken to avoid collecting samples with evidence of solid-state deformation so that the AMS results reflect solely magmatic fabric. Each of these hand samples was cored in the laboratory. These 25 mm diameter cores were oriented and cut into 22 mm-long specimens. Because the igneous rock of the Maiden Creek intrusion is porphyritic, small-scale fabric variations are expected due to the relatively small number of phenocrysts within each specimen. Therefore, an effort was made to ensure that six or more specimens were created and analyzed for each hand sample in order to strengthen statistical analysis of the data. Low-field AMS was measured on each specimen with a Kappabridge KLY-3S susceptibility bridge at the University of Wisconsin-Madison. Results for each sample were compiled using the AniSoft software package supplied with the Kappabridge.

4.4.2. Magnetic mineralogy

The magnetic mineralogy of the Maiden Creek porphyry was investigated at the University of Minnesota's Institute for Rock Magnetism. Fig. 8a is a plot of susceptibility vs. temperature showing that the magnetic signal is dominated by magnetite (Curie $T\approx570$ °C). Fig. 8b is a Day plot (Day et al., 1977) indicating that the porphyry's magnetic mineralogy is dominated by multi-domain magnetite. AMS results therefore reflect the SPO of the magnetite grains within the porphyry (Grégoire et al., 1995; Borradaile and Henry, 1997). Consequently, K_1 can be interpreted as the magnetic lineation and K_3 as the pole to the magnetic foliation plane (e.g. Rochette et al., 1992; Ferré, 2002).

Many thin sections of the porphyry show some evidence of alteration. Amphibole is most affected by this alteration and is often replaced by a combination of oxides, epidote, chlorite and calcite. Feldspar phenocrysts are altered to sericite and fine-grained feldspar along fractures and cleavage planes (Hunt, 1953; Engel, 1959). Engel (1959) concluded that most of this alteration is the result of deuteric reactions of the porphyry with the last volatile phase that

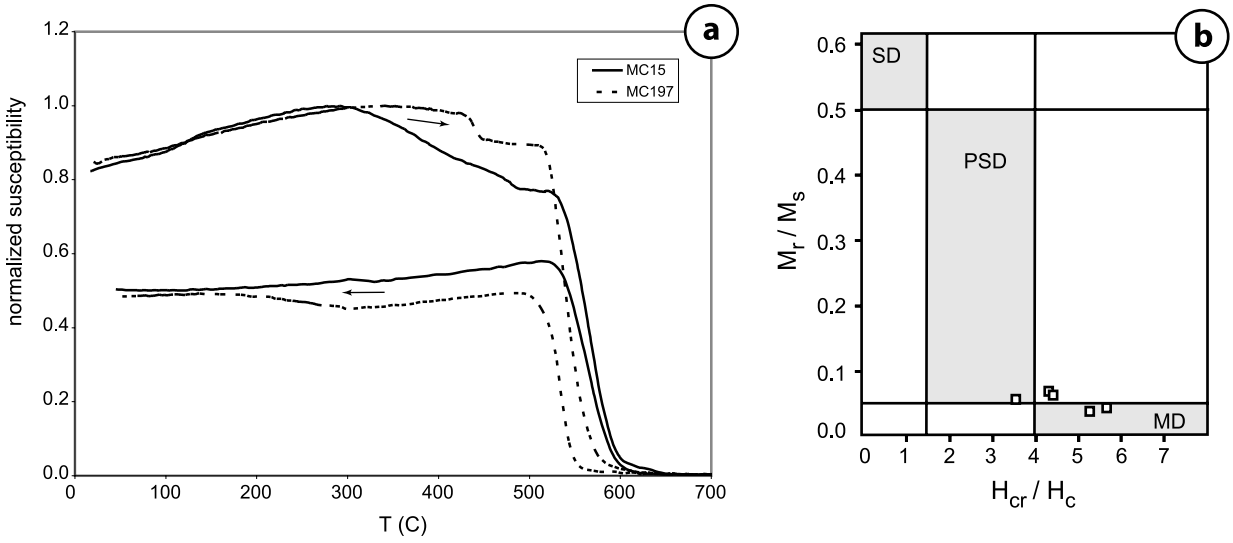

Fig. 8. (a) A plot of susceptibility vs. temperature for two samples of the Maiden Creek porphyry. Arrows indicate directions of heating and cooling. The susceptibility of both samples is dominated by magnetite. (b) A Day plot for determination of magnetic domain grain size where MD = multi-domain, PSD = pseudo-single domain, SD = single domain magnetite. The results for five samples from the Maiden Creek intrusion (open squares) indicate that the magnetite in these samples is primarily multi-domain.

remained after emplacement and solidification. The alteration of amphibole to oxides (principally magnetite) controls the secondary oxide SPO and is therefore of particular importance for consideration of AMS results because of the high susceptibility of many oxides.

4.4.3. Results

Orientation results of the AMS analysis are presented in Figs. 9–11. The K, T,and P' parameter results are presented in Fig. 12. For comparison with other fabric determination techniques, results from the AMS analysis for the pertinent stations are plotted on Fig. 7. Interpretation and discussion of AMS results relative to the other fabric determination techniques is given in Section 4.5.

Away from the margins of the intrusion, magnetic foliation tends to be roughly subhorizontal (Fig. 11). Near the margins of each sheet, the magnetic foliation tends to be sub-parallel to the contact, regardless of the orientation of the margin. This contact-parallel orientation is most obvious near the bulbous termination of the igneous sheets (Fig. 9). These broad patterns of magnetic foliation are observed in both the main body and the fingers of the intrusion.

Magnetic lineation in the interior of the main body of the sill is consistently subhorizontal and tends to radiate roughly perpendicularly to the margin of the main body. Lineation patterns in the fingers of the sill are distinct from those observed in the main body. In the interior of each finger, away from the margins, lineations tend to be subhorizontal (Figs. 10 and 11). Lineation trends in each finger display a radial pattern suggesting flow out of the main body and into the finger. This radial pattern tends to make an angle of 30–40° with the nearest lateral margin of the finger. The plunge of magnetic lineation near bulbous terminations shows a complex relationship similar to that observed near bulbous terminations in the main body. These lineations are considered further in Section 5.

The bulk susceptibility (K_b) of the samples ranges from 310 to 15095 μSI (Fig. 12). No spatial pattern of K_b values within the sill is apparent, but thin section analysis indicates that the lowest K_b values are from samples that have experienced a large amount of post-emplacement alteration. Magnetite in these samples has been replaced by other less magnetic minerals.

The positive T-values observed throughout the sill (Fig. 12) indicate a general oblate shape of the magnetic fabric within the intrusion, suggesting that fabrics are dominated by foliation (flattening) rather than lineation (constriction).

Values of the degree of anisotropy (P') for the Maiden Creek sill range from 1.016 to 1.062 (Fig. 12), indicating a fairly low degree of anisotropy typical of magmatic fabrics developed in granitic rocks (e.g. de Saint-Blanquat and Tikoff, 1997; Becker et al., 2000; Sant'Ovaia et al., 2000; Steenken et al., 2000). Stations with high degrees of anisotropy generally have very positive T-values (Fig. 12(e)). In contrast, stations with prolate fabrics generally have a relatively low degree of anisotropy.

4.5. Comparison of results from different techniques

As Fig. 7 shows, there is broad agreement on fabric orientation within each sample as determined with these different techniques. Foliation orientation, in particular, is generally consistent between all of the techniques; poles to foliation (short axes) determined with different techniques agree with one another within ±20°. Lineation orientation is less consistently determined between the different

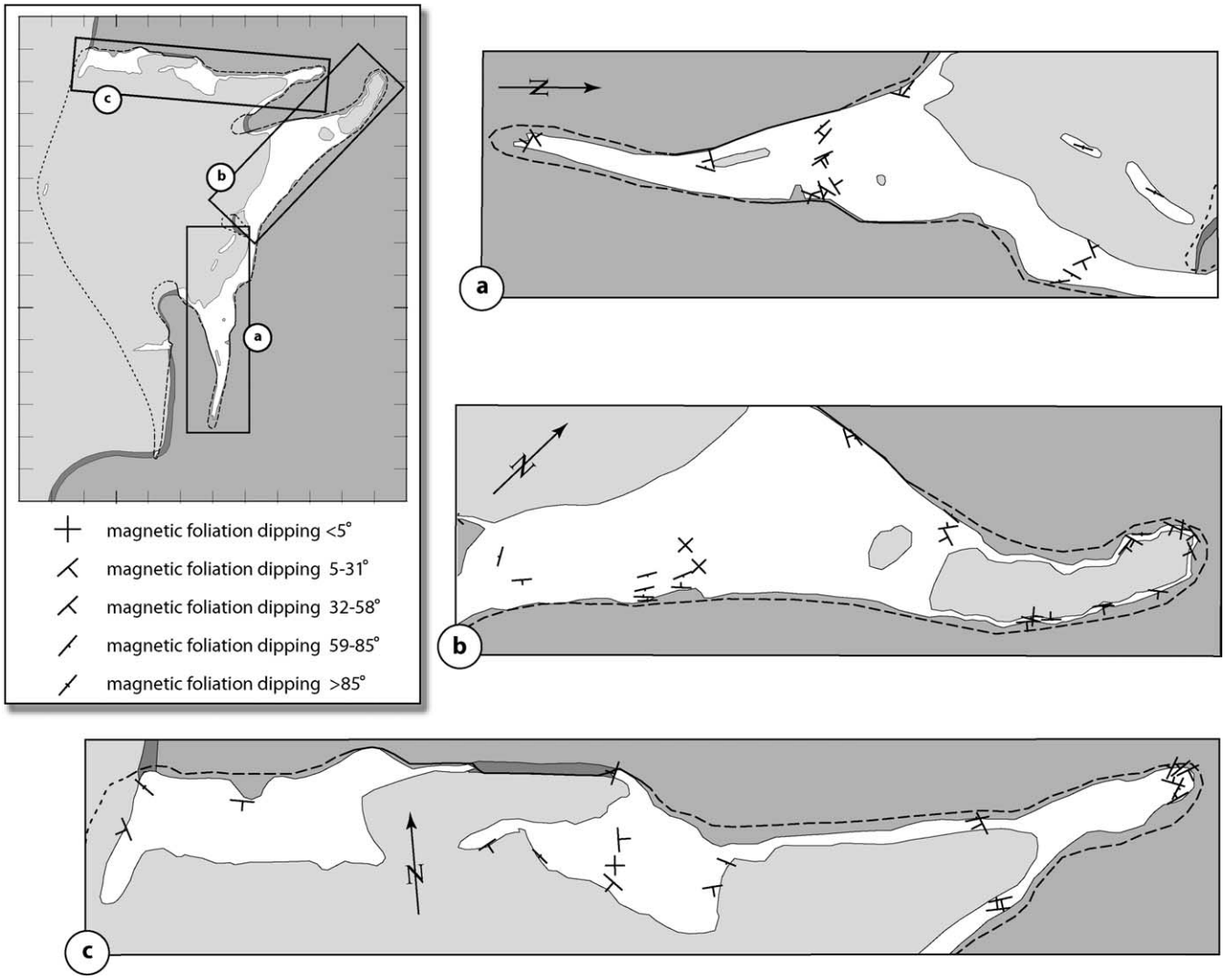

Fig. 9. Magnetic foliation results plotted on geological strip maps. Strip map locations are given on the inset geological map of the Maiden Creek sill. See Fig. 2 for map unit legend.

techniques, although all results generally agree with measured field lineation. X-ray CT orientation results, in particular, are different from results obtained from the other analysis techniques. We ascribe this inconsistency to the combination of small sample size analyzed for CT and the porphyritic nature of the rock. Together these factors result in the calculation of an SPO based on a small number of crystals, with the result that orientations are relatively poorly determined.

Within the results for any one technique, fabric ellipsoid orientations for different clast populations disagree. Phases with relatively large aspect ratios better reflect the deformation of the magma because they tend to rotate into parallelism with the principal finite strain axes (Ghosh and Ramberg, 1976; Passchier, 1987; Jezek et al., 1996), which are here caused by magmatic flow. Within the Maiden Creek sill, amphibole phenocrysts have the largest aspect ratio and thus provide the best record of finite strain caused by magmatic flow.

The different fabric determination techniques analyze different parts of the rock mass, consider different mineral phases, and have different scales of resolution. The techniques also measure different physical properties of the specimens. Image analysis and X-ray CT techniques determine and quantify, at different scales, the SPO of mineral grains. In contrast, AMS is a measure of the magnetic properties of the rock. Despite the different characteristics being measured, results from the different fabric determination techniques broadly agree on bulk fabric orientation. However, the variability of fabric results observed here with the different techniques suggests that it is advisable to avoid relying upon a single fabric measurement technique and that, due to the assumptions inherent within and the different rock characteristics measured by a given technique, care must be taken in the interpretation of any fabric data. When using multiple fabric techniques, observations consistent between all techniques are the most robust and most reliable.

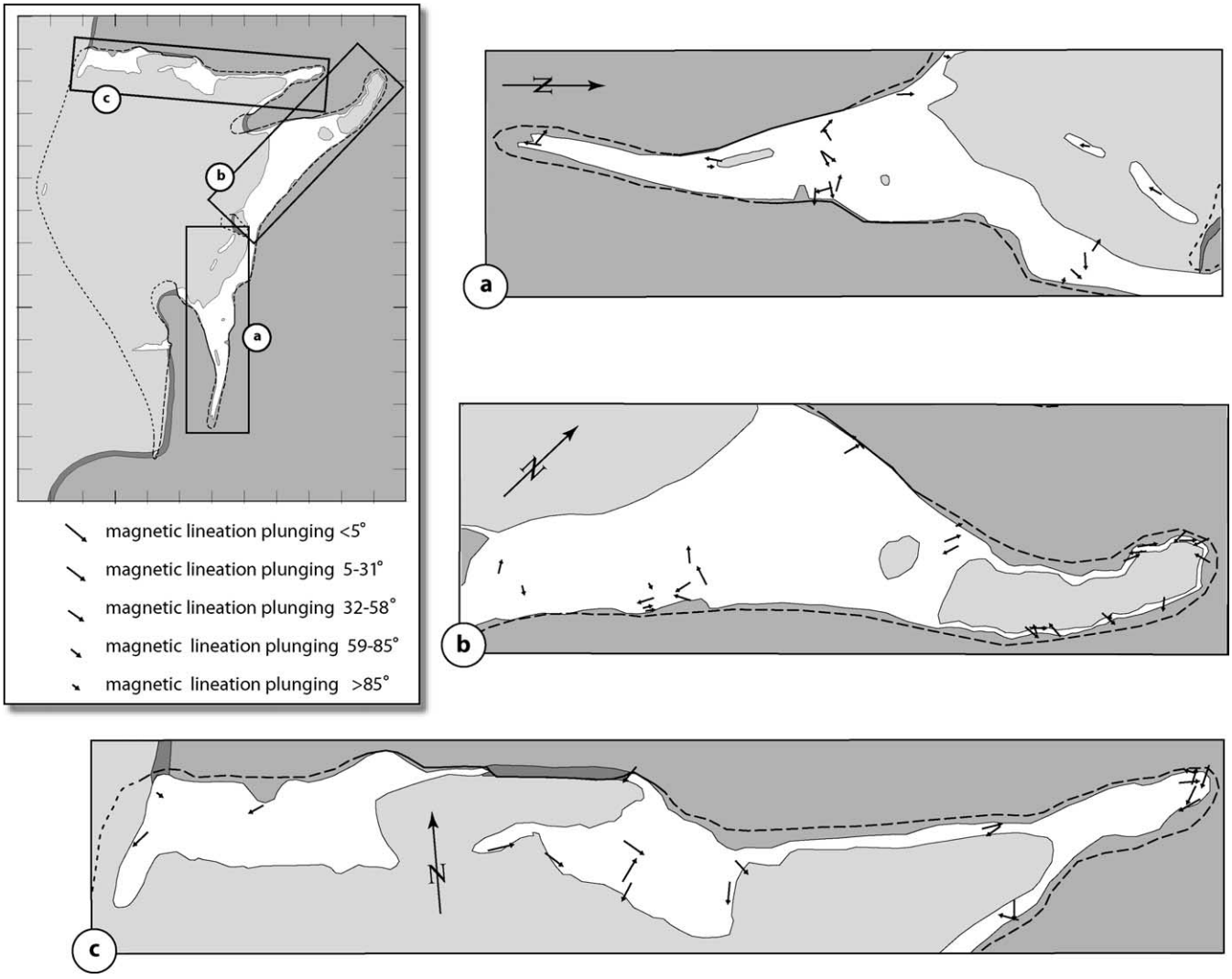

Fig. 10. Magnetic lineation results plotted on geological strip maps. Strip map locations are given on the inset geological map of the Maiden Creek sill. See Fig. 2 for map unit legend.

The broad agreement on bulk fabric orientation observed here between the techniques lends further support to the contention that AMS, carefully interpreted, is a good indicator of magmatic fabric (Knight and Walker, 1988; Rochette et al., 1992; Tarling and Hrouda, 1993; Borradaile and Henry, 1997; Bouchez, 1997; Launeau and Cruden, 1998). The ease and speed with which AMS can be measured makes this technique particularly useful for the collection of large data sets. Consequently, much of the following discussion of fabric in the Maiden Creek intrusion will focus on the AMS results.

5. Discussion

5.1. Interpretation of fabric data

5.1.1. Internal fabric

The fabric patterns observed in the interior of the intrusion are consistent with emplacement away from a feeder west of the current exposure, toward the center of the Mt Hillers intrusive complex. The subhorizontal foliation probably records the flattening that occurred during emplacement as magma flowed away from the feeder and simultaneously lifted the overburden to make room for the intrusion. This flattening fabric is corroborated by the dominantly positive *T*-values recorded in the AMS measurements throughout the main body.

5.1.2. Margin fabric and opposing shear sense

In cross-sections away from the lateral margins of the intrusion, foliation obliquity is opposite at the upper and lower contacts of the intrusion, indicating opposite senses of shear at these contacts. This geometry implies that the center of each igneous sheet flowed more rapidly than the edges (Fig. 13). A similar pattern has been observed in a wide variety of field studies of sheet intrusion emplacement

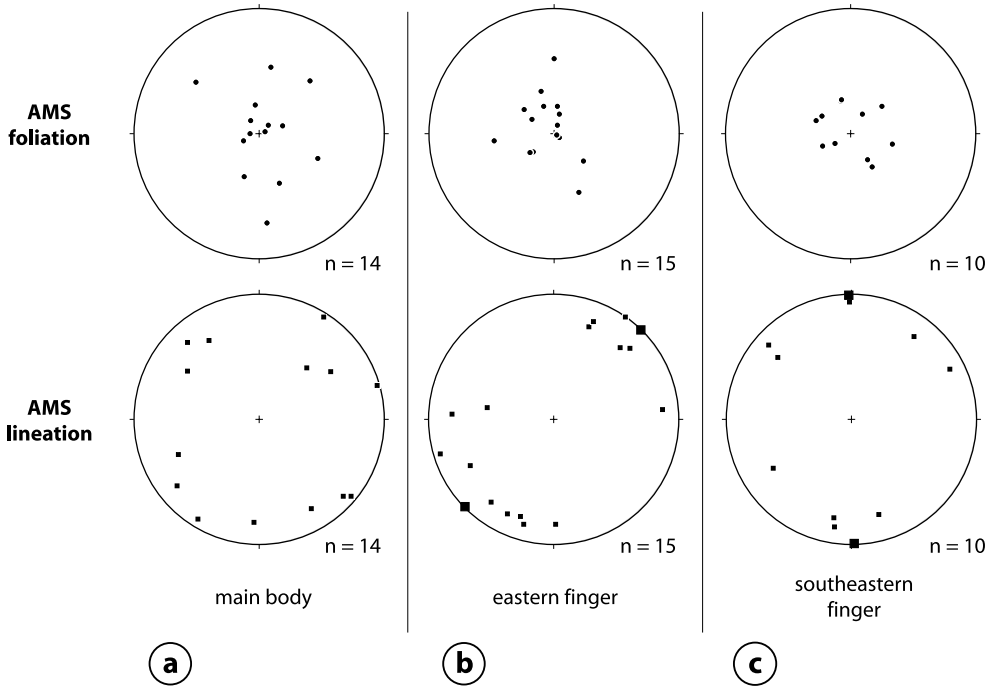

Fig. 11. AMS foliation and lineation results from regions of the sill plotted on equal angle lower hemisphere stereographic projections. The results shown here are from stations greater than 1 m from the nearest contact and are intended to show the broad fabric patterns in the interior of the intrusion. (a) AMS results from the interior of the main body of the intrusion. Foliations are generally subhorizontal. Lineations trend radially and plunge shallowly. (b) AMS results from the interior of the easternmost finger of the intrusion. These results are from both the interior and on top of the finger. Foliations are generally subhorizontal. Lineations plunge shallowly and have trends varying $\pm$30–40° to the long axis of the finger (large squares). (c) AMS fabric results from the interior of the southeastern finger of the intrusion. These results are from stations in the interior and on top of the finger. Foliations are generally subhorizontal. Lineations plunge shallowly and have trends varying $\pm$30–40° to the long axis of the finger.

(e.g. Komar, 1972, 1976; Ross, 1986; Wada, 1992; Correa-Gomes et al., 2001).

In general, fabric near an intrusion contact in the Maiden Creek sill is significantly better developed than away from the contact. This increase in fabric strength can be attributed to the higher finite strain due to drag of the magma against the margin of the intrusion. At a particular location, the solid-state fabric presumably develops relatively early in the emplacement history before the wall rock is appreciably heated. In the Maiden Creek intrusion, the increase in fabric intensity toward the margins is documented by the degree of magnetic anisotropy (Fig. 12), with the highest values of P' occurring less than 1 m from the nearest margin. Although the margins appear to affect the bulk susceptibility and degree of anisotropy parameters (presumably due to late alteration), the shape of the AMS ellipsoids throughout the sill is consistently oblate and has no clear relationship to the margins of the intrusion.

5.1.3. Fanning lineation patterns

Two radial lineation patterns are observed in the Maiden Creek sill: one within the main body of the intrusion and another within the finger-like lobes. The radial pattern in the main body records some component of the magmatic flow direction during emplacement of the main body, in relation to the location and geometry of the intrusion's feeder system. Although the feeder for the Maiden Creek intrusion is not exposed, the lineation pattern suggests that it should be located to the west or southwest of the intrusion, in the direction of the Mt Hillers intrusive center (Fig. 1).

In the fingers, the general alignment of the lineation with the elongation of the fingers suggests flow from the main body out into the fingers. However, the lineation tends to make a small angle (generally less than $\sim$30°) with the nearest lateral margin of the finger (Fig. 13). We interpret this consistent obliquity to form as a result of the fingers growing simultaneously in width and length during emplacement. The presence of fabric rotation on the edges of the intrusion suggests that magma velocity is slower on the edges of the intrusion than in the middle. Within the fingers, however, this drag effect is three-dimensional (Fig. 13), rather than two-dimensional as outlined above, because the finger-like lobes are relatively narrow and thin. Consequently, we infer that magmatic flow is fastest in the middle of the finger.

5.2. Emplacement

In this section, we attempt to integrate the three-dimensional geometry of the pluton, fabric data, and inferences about magmatic flow to provide a model for the emplacement of the Maiden Creek sill.

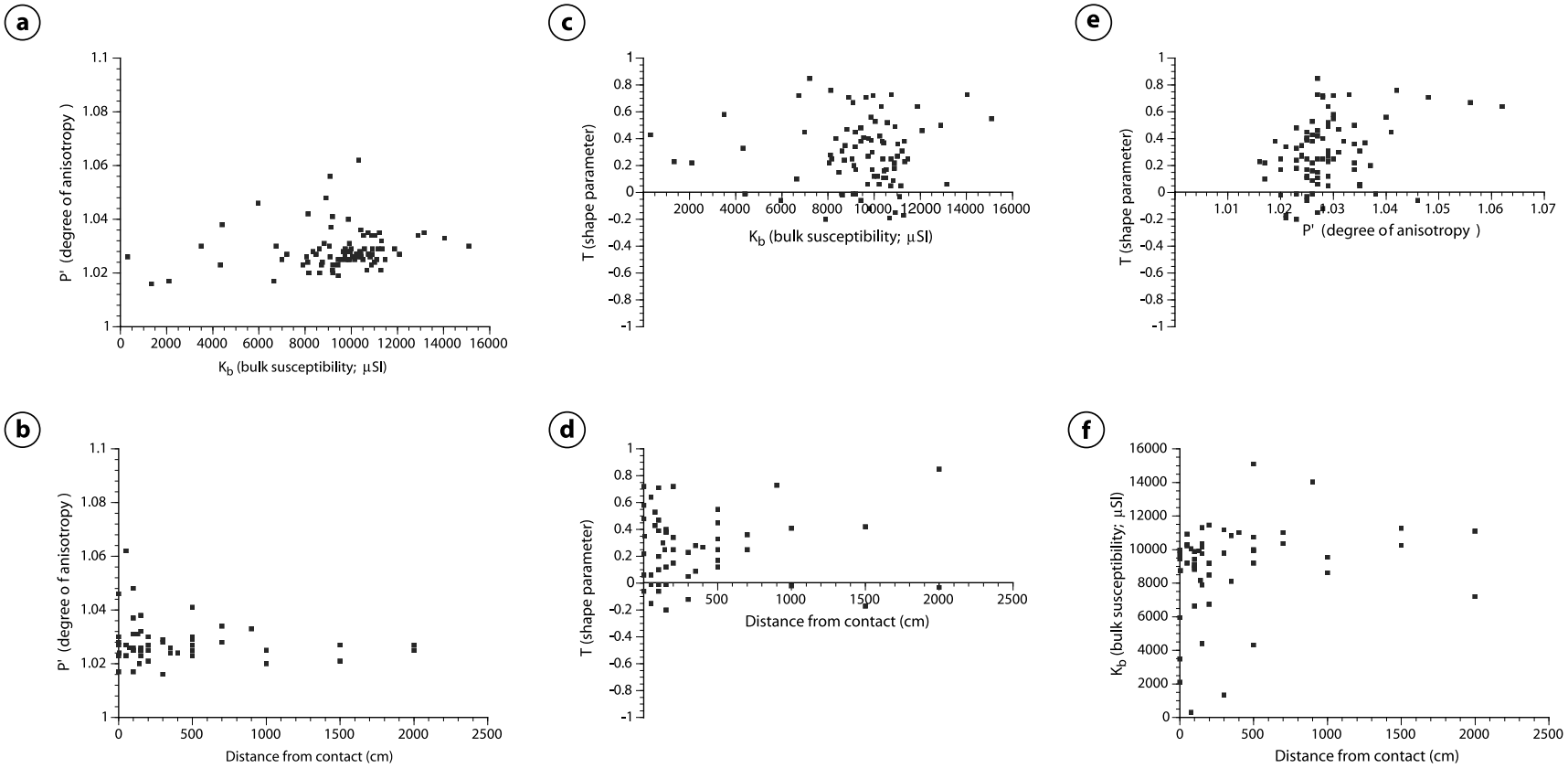

Fig. 12. Plots of AMS parameters. (a) Degree of anisotropy vs. bulk susceptibility. (b) Degree of anisotropy vs. distance of station from contact with wall rock. (c) Shape parameter vs. bulk susceptibility. (d) Shape parameter vs. distance of station from contact. (e) Shape parameter vs. degree of anisotropy. (f) Bulk susceptibility vs. distance of station from contact.

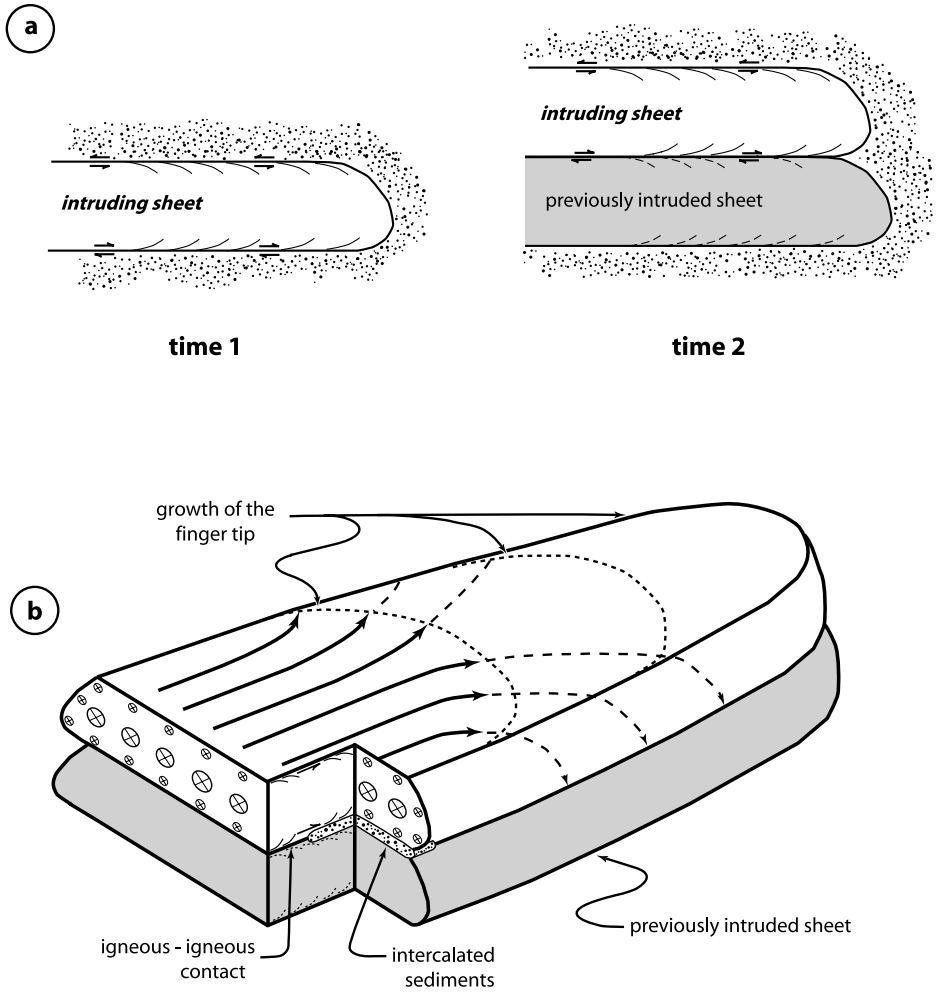

Fig. 13. Diagrammatic sketches of the emplacement of the Maiden Creek sill. (a) The sill was emplaced as two separate sheets of igneous material, one shortly after the other. Sense of shear is indicated by fabric obliquity and is opposite on the top and bottom of a sheet. (b) Schematic model of emplacement of the second sheet in a finger-like lobe of the intrusion. See main text for explanation of the model. The solid outline corresponds to the final finger geometry, which narrows along its length. Arcuate dashed lines on top of the finger correspond to the tip of the lobe at different stages during progressive emplacement. On the rear of the emplacing sheet, the size of arrow tails corresponds to magma velocity; material flows faster in the center of the sheet than at the edges. Sense of shear within the emplacing sheet is indicated by fabric obliquity. On the top and sides of the emplacing sheet, solid and dashed arrows show lineation trends and roughly describe material flow paths, which progressively produce the fabric patterns observed in the field.

5.2.1. Fingers

Finger-like lobes have been noted in other intrusions, such as Trachyte Mesa, Shonkin Sag laccolith (Highwood Mountains, Montana), and the La Veta dikes near La Veta, Colorado (Pollard et al., 1975). The Maiden Creek sill fingers are distinctive in a variety of ways. (1) They are far fewer in number with respect to the intrusion's size than what was observed at the other locations. (2) They are significantly larger with respect to intrusion size than those observed elsewhere ~200–400 m long compared with 1–10 m (Trachyte Mesa, Shonkin Sag). (3) They are each composed of at least two separate intrusive sheets.

Pollard et al. (1975) used magma viscosity differences to explain different finger geometries observed at various locations. In particular, the short (1–3 m), wide fingers observed at Trachyte Mesa, were interpreted as a product of the very high viscosity of the Henry Mountains porphyry. The Trachyte Mesa intrusion is adjacent to Maiden Creek sill and is very similar in composition, yet the length-to-width aspect ratios of the two intrusions' fingers are significantly different. Thus, viscosity alone is not sufficient to explain finger geometry. We cannot distinguish between two possible relationships between the fingers and the main body of the Maiden Creek intrusion. (1) The main body may be a region that has coalesced into a sheet of magma behind several propagating fingers, as described by Pollard et al. (1975). (2) The fingers may be ancillary small intrusions fed by the main body, rather than the distal propagating edge of a larger sheet intrusion.

Regardless of the relationship between the fingers and the main body, the initiation of the fingers likely occurred in a manner similar to that proposed by Pollard et al. (1975). Each finger probably initiated at the margin of a relatively small body of magma as a small protuberance, perhaps due

to a local inhomogeneity such as a fracture set in the nearby sediments. The pressure within this protuberance drove its walls out away from the main magma body, which then served as the feeder for the fingers as they propagated radially away. This propagation continued until the magma at the margin of the finger no longer had sufficient driving pressure to continue lifting adjacent sediments.

The lineations preserved on top of the intrusion and in bulbous terminations are consistent with the progressive propagation of each finger by this mechanism. Thus, both the solid-state and magmatic fabric near intrusion margins record information about the complex magmatic flow that formed in these regions of the intrusion as a consequence of the propagating margin (Fig. 13).

5.2.2. Spatial coincidence of magma pulses

As discussed earlier, we infer that the Maiden Creek sill consists of two separate, sequentially emplaced sheets. These sheets have identical cross-sectional geometry and areal extent so the magma pulses that fed the sheets were essentially identical in volume and presumably had similar driving pressure. The sheets' identical areal extent suggests that the emplacement and extent of the first sheet controlled the extent of the second sheet.

We envision the following scenario. The emplacement of the first sheet produced a weak, hot region surrounding the igneous body. During intrusion of subsequent igneous sheets, this weak region was preferentially exploited. Consequently, after the emplacement of the first sheet, subsequent pulses of magma from the same feeder system intruded immediately adjacent to the previously intruded sheet. By this process, a sheeted body of igneous rock with a complex lobate three-dimensional geometry is built, while the amount of magma intruding at any one time remains small.

Similar sheeted emplacement processes have been observed in larger plutons. Hutton (1992) observed sheeted plutons in transcurrent, extensional, and contractional tectonic settings and concluded that the emplacement of these plutons was controlled by multiple sheets of magma, regardless of tectonic setting. Barton et al. (1995) mapped the Birch Creek pluton in detail and observed that it had coalesced from multiple magmatic sheets. Based on fabric observations of the Tuolumne Intrusive Suite and thermal modeling of igneous emplacement processes, Glazner et al. (2004) suggest that large plutons can form through the incremental accumulation of many small igneous bodies. Rocchi et al. (2002) studied several laccoliths on the Isle of Elba in Italy and concluded that the km-scale intrusions were formed by the amalgamation of relatively small sheet-like igneous bodies.

Our study area, because of its relative simplicity, allows us both to recognize sheeted emplacement in a small intrusion and to examine how sheets coalesce. It appears that some feedback mechanism exists between the initial emplacement of an intrusive sheet and subsequently emplaced sheets. This feedback relationship may be important for emplacement of plutons over a wide range of scales and depths.

6. Conclusions

The Maiden Creek intrusion has a complex three-dimensional geometry. The main body of the intrusion is roughly elliptical in map view and has a relatively simple sill-like geometry in cross-section. This region of the intrusion is consistently 30–40 m thick. At least four separate, finger-like lobes project out from this main body. Each of these fingers is approximately 30–40 m thick where it begins to project out from the main body and thins progressively to a thickness of 5–10 m as distance from the main body increases. These fingers extend 200–400 m out from the main body of the intrusion and are distinctly elongate with respect to both their map view width and their cross-sectional thickness.

The Maiden Creek intrusion is composed of at least two separate, sequentially emplaced igneous sheets, each essentially identical in composition, thickness and areal extent. Several features are useful to distinguish these two sheets. (1) Intense solid-state fabric develops locally at sheet contacts. (2) Sediments are sometimes intercalated between separate igneous sheets. (3) A bulbous termination forms at each lateral sheet margin. These bulbous terminations are very consistent in their size and geometry, regardless of whether they develop at the lateral margin of the main body of the intrusion or at the lateral margin of a finger-like lobe.

Magmatic and solid-state fabrics within the intrusion were determined with field measurements, SPO analysis by both image analysis and X-ray CT, and AMS. We observed a clear relationship between fabric development and intrusion contacts. In the internal parts of the intrusion, away from the margins, fabric is magmatic, with weak subhorizontal foliation and lineation. Near the contacts of the intrusion, magmatic fabric strength progressively increases and fabric orientation becomes more contact parallel. At distances generally less than 15 cm from the contact of the intrusion with adjacent wall rock, solid-state fabric begins to overprint the magmatic fabric. This solid-state fabric progressively increases in strength and becomes more contact parallel as distance from the contact decreases. Shear sense consistently indicates that magma flowed more rapidly in the interior of the intrusion than near the margins. Because the strongest fabrics in the sill are consistently developed near the exposed contacts of the intrusion, contacts with wall rock are often recognizable even when sediments have eroded away.

The internal subhorizontal flattening fabric and deformation of the overlying rock suggests that each sheet was forcefully emplaced by uplift of the overlying sediments. We hypothesize that the close correspondence of the sheet geometries exists because the geometry of the first sheet

controlled the geometry of the second, probably through thermal and/or strength anisotropy imparted to the system by emplacement of the first sheet. We conclude that sheeted emplacement can be an important process in small intrusions and speculate that sheeted emplacement observed in larger intrusions may initiate and continue through processes like those described here.

Acknowledgements

We thank Michel de Saint-Blanquat, Guillaume Habert, Karoun Charkoudian and Beverley Shade for field assistance. Dave Dilloway and the Hanksville B.L.M. office provided essential logistical assistance. Richard Ketcham performed the X-ray CT analysis at the University of Texas, Austin High Resolution X-ray Computed Tomography facility. We also thank Jean-Luc Bouchez and Scott Paterson for critical reviews that greatly improved this manuscript. Funding for this work was provided by National Science Foundation grant EAR-0003574.

Appendix A. X-ray computed tomography

This appendix provides a brief overview of the theory and process of the X-ray computed tomography analysis techniques and is summarized from Herman (1980), Wellington and Vinegar (1987), Flannery et al. (1987) and Denison et al. (1997). The velocity of an X-ray traveling through any material depends on the X-ray attenuation of that material. The degree to which an X-ray's velocity is attenuated by a substance is predominantly a function of the density of that substance. Thus, by measuring the time it takes an X-ray to travel through an object of known dimensions, the average density of the object along the path of the X-ray can be calculated. By combining the results from many different X-ray paths and iteratively solving for attenuation variation, the density distribution within the object is mapped in three dimensions.

Like any tomographic procedure, X-ray CT analysis begins with the construction of a theoretical model of the object to be mapped. This model is discretized into numerous cells, each of which is assigned a value for the parameter to be modeled (e.g. density or attenuation). As data are collected, the values of the parameter in each cell within the model are progressively improved to better fit the observations.

Data are gathered in a series of thin slices through the object. In order to analyze a slice, the object is placed on a turntable and a beam of X-rays is directed through it. The velocity and corresponding attenuation of each X-ray is calculated. This observed velocity for each X-ray path is compared with the expected velocity for the same path as calculated from the theoretical attenuation model. Initially the expected and observed results do not agree. Consequently, the cells within the theoretical model through which the X-ray traveled are modified to fit the observed data. This process is repeated for each X-ray. The object is then rotated on the turntable and another beam of X-rays is sent through the object, their velocities are analyzed, and the model is adjusted to better fit the observations. This process continues until the theoretical attenuation model provides a good match for all of the observed X-ray velocities along this slice through the object. Once this point has been reached, the theoretical model is a good approximation of the attenuation (i.e. density) geometry of the thin slice being analyzed.

Many of these pseudo-two-dimensional (each slice is $\sim$50 μm thick in the samples analyzed for this study) slices are stacked to create the three-dimensional density distribution within the object. From the stacked results, the bulk orientation for each separate density phase is analyzed. These orientation calculations involve randomly distributing reference points in the phase of interest throughout the stacked data. At each reference point, the shape of the region in which the reference point is located is calculated by measuring the distance to a change in density (e.g. a different phase) in many radial directions. Thus, each object is effectively mapped in three dimensions. Orientations of the different phases are calculated using the star volume distribution (SVD) method, which uses infinitesimal cones to measure the distance to a density change. The 'star' designation refers to the spherical radiation of measurement directions surrounding each reference point.

From the results of each of these methods, a second-rank tensor is calculated that describes the bulk orientation and distribution of each population of different density material within the object. The eigenvectors and corresponding eigenvalues of this tensor define the principal axes of an SPO ellipsoid that can be used to describe the bulk orientation of the phase in question.

References

Barton, M., Ghidotti, G., Holden, P., Goodwin, L., Heizler, M., 1995. Time–space evolution of a two-mica granite; the Birch Creek Pluton, CA, USA. In: Brown, M., Piccoli, P. (Eds.), The Origin of Granites and Related Rocks U.S.G.S. Circular, 1129, pp. 18–19.

Becker, J.K., Siegesmund, S., Jelsma, H.A., 2000. The Chinamora batholith, Zimbabwe: structure and emplacement-related magnetic rock fabric. Journal of Structural Geology 22, 1837–1853.

Benn, K., Allard, B., 1989. Preferred mineral orientations related to magnetic fabric in ophiolite layered gabbros. Tectonophysics 233, 153–162.

Blanchard, J.P., Boyer, P., Gagny, C., 1979. Un nouveau critere de sens de mise en place dans une caisse filonienne: le "pincement" des mineraux aux epontes. Tectonophysics 53, 1–25.

Borradaile, G., 1988. Magnetic susceptibility, petrofabrics and strain. Tectonophysics 156, 1–20.

Borradaile, G., Henry, B., 1997. Tectonic applications of magnetic susceptibility and its anisotropy. Earth Science Reviews 42, 49–93.

Bouchez, J.-L., 1997. Granite is never isotropic: an introduction to AMS studies of granitic rocks. In: Bouchez, J.-L., Hutton, D.H.W., Stephens, W.E. (Eds.), Granite: from Segregation of Melt to Emplacement Fabrics. Kluwer, Dordrecht, pp. 95–112.

Bouchez, J.L., Delas, C., Gleizes, G., Nedelec, A., Cuney, M., 1992. Submagmatic microfractures in granites. Geology 20, 35–38.

Correa-Gomes, L.C., Souza Filho, C.R., Martins, C.J.F.N., Oliveira, E.P., 2001. Development of symmetrical and asymmetrical fabrics in sheet-like igneous bodies: the role of magma flow and wall-rock displacements in theoretical and natural cases. Journal of Structural Geology 23, 1415–1428.

Corry, C., 1988. Laccoliths: Mechanics of Emplacement and Growth, Geological Society of America Special Paper, vol. 110 1988. 110pp.

Day, R., Fuller, M., Schmidt, V.A., 1977. Hysteresis properties of titanomagnetites: grain-size and compositional dependence. Physics of the Earth and Planetary Interiors 13, 260–267.

Denison, C., Carlson, W.D., Ketcham, R.A., 1997. Three-dimensional quantitative textural analysis of metamorphic rocks using high-resolution computed X-ray tomography: Part I. Methods and techniques. Journal of Metamorphic Geology 15, 29–44.

de Saint-Blanquat, M., Tikoff, B., 1997. Development of magmatic to solid-state fabrics during syntectonic emplacement of the Mono Creek granite, Sierra Nevada batholith. In: Bouchez, J.L., Hutton, D.H.W., Stephens, W.E. (Eds.), Granite: from Segregation of Melt to Emplacement Fabrics. Kluwer, Dordrecht, pp. 231–252.

Engel, C.G., 1959. Igneous rocks and constituent hornblendes of the Henry Mountains, Utah. Geological Society of America Bulletin 70, 951–980.

Ferré, E.C., 2002. Theoretical models of intermediate and inverse AMS fabrics. Geophysical Research Letters 29.

Flannery, B.P., Deckman, H.W., Roberge, W.G., D'Amico, K.L., 1987. Three-dimensional microtomography. Science 237, 1439–1444.

Ghosh, S.K., Ramberg, H., 1976. Reorientation of inclusions by a combination of pure and simple shear. Tectonophysics 34, 1–70.

Gilbert, G.K., 1877. Geology of the Henry Mountains, Utah. US Geographical and Geological Survey of the Rocky Mountain Region, 170pp.

Glazner, A.F., Bartley, J.M., Coleman, D.S., Gray, W., Tayler, R.Z., 2004. Are plutons assembled over millions of years by amalgamation from small magma chambers? G.S.A. Today 14 doi: 10.1130/1052-5173(2004)013<0004:APAOMO>.

Grégoire, V., de Saint-Blanquat, M., Nédélec, A., Bouchez, J.-L., 1995. Shape anisotropy versus magnetic interaction and application to AMS in granitic rocks. Geophysical Research Letters 20, 2765–2768.

Habert, G., de Saint-Blanquat, M., 2004. Rate of construction of the Black Mesa bysmalith, Henry Mountains, Utah, USA. In: Breitkreutz, C. and Petford, N. (eds.) Physical geology of high-level magmatic systems. Geological Society of London Special Publication 234: 143–159.

Herman, G.T., 1980. Image Reconstruction from Projections: The Fundamentals of Computerized Tomography, vol. 316. Academic Press, New York.

Hrouda, F., 1982. Magnetic anisotropy of rocks and its application in geology and geophysics. Geophysical Surveys 5, 37–82.

Hunt, C., 1953. Geology and geography of the Henry Mountains region, Utah. US Geological Survey Professional Paper 228, 234pp.

Hutton, D.H.W., 1988. Granite emplacement mechanisms and tectonic controls: inferences from deformation studies. Transactions of the Royal Society-Edinburgh 79, 245–255.

Hutton, D.H.W., 1992. Granite sheeted complexes: evidence for the diking ascent mechanism. Transactions of the Royal Society-Edinburgh 83, 377–382.

Jackson, M., Pollard, D., 1988. The laccolith-stock controversy: new results from the southern Henry Mountains, Utah. Geological Society of America Bulletin 100, 117–139.

Jezek, J., Schulmann, K., Segeth, K., 1996. Evolution of rigid inclusions during mixed coaxial and simple shear flows. Tectonophysics 257, 203–221.

Johnson, A.M., Pollard, D.D., 1973. Mechanics of growth of some laccolithic intrusions in the Henry Mountains, Utah, Part I: Field observations, Gilbert's model, physical properties and flow of the magma. Tectonophysics 18, 261–309.

Knight, M.D., Walker, G.P.L., 1988. Magma flow direction in dykes of the Koolau complex, Oahu, determined from magnetic fabric studies. Journal of Geophysical Research 93, 4301–4319.

Komar, P.D., 1972. Flow differentiation in igneous dikes and sills: profiles of velocity and phenocrysts concentration. Geological Society of America Bulletin 83, 3443–3448.

Komar, P.D., 1976. Phenocryst interactions and the velocity profile of magma flowing through dikes and sills. Geological Society of America Bulletin 87, 1336–1342.

Launeau, P., Cruden, A.R., 1998. Magmatic fabric acquisition in a syenite: results of a combined anisotropy of magnetic susceptibility and image analysis study. Journal of Geophysical Research 103, 5067–5089.

Launeau, P., Robin, P.F., 1996. Fabric analysis using the intercept method. Tectonophysics 267, 91–119.

Launeau, P., Robin, P.F., 2001. Ellipsoid2001. Available upon request from P. Launeau: http://www.sciences.univ-nantes.fr/geol/UMR6112/Persnl/launeau.html.

Launeau, P., Bouchez, J.L., Benn, K., 1990. Shape preferred orientation of object populations: automatic analysis of digitized images. Tectonophysics 180, 201–211.

Nelson, S.T., Davidson, J.P., Sullivan, K.R., 1992. New age determinations of central Colorado Plateau laccoliths, Utah: Recognizing disturbed K–Ar systematics and re-evaluating tectonomagmatic relationships. Geological Society of America Bulletin 104, 1547–1560.

Passchier, C.W., 1987. Stable positions of rigid objects in non-coaxial flow: a study in vorticity analysis. Journal of Structural Geology 9, 679–690.

Paterson, S.R., Fowler Jr., T.K., Schmidt, K.L., Yoshinobu, A.S., Yuan, E.S., Miller, R.B., 1998. Interpreting magmatic fabric patterns in plutons. Lithos 44, 53–82.

Pollard, D.D., Johnson, A.M., 1973. Mechanics of growth of some laccolithic intrusions in the Henry Mountains, Utah, Part II: Bending and failure of overburden and sill formation. Tectonophysics 18, 311–354.

Pollard, D.D., Muller, O.H., Dockstader, D.R., 1975. The form and growth of fingered sheet intrusions. Geological Society of America Bulletin 3, 351–363.

Ramsay, J.G., 1980. Shear zone geometry: a review. Journal of Structural Geology 2, 83–101.

Robin, P.F., 2002. Determination of fabric and strain ellipsoids from measured sectional ellipses—theory. Journal of Structural Geology 24, 531–544.

Rocchi, S., Westernman, D.S., Dini, A., Innocenti, F., Tonarini, S., 2002. Two-stage growth of laccoliths at Elba Island, Italy. Geology 30, 983–986.

Rochette, P., Jackson, M., Aubourg, C., 1992. Rock magnetism and the interpretation of anisotropy of magnetic susceptibility. Reviews of Geophysics 30, 209–226.

Ross, M.E., 1986. Flow differentiation, phenocrysts alignment, and compositional trends within a dolerite dike at Rockport, Massachusetts. Geological Society of America Bulletin 97, 232–240.

Sant'Ovaia, H., Bouchez, J.-L., Noronha, F., Leblanc, D., Vigneresse, J.-L., 2000. Composite-laccolith emplacement of the post-tectonic Vila Pouca de Aguiar granite pluton (northern Portugal): a combined AMS and gravity study. Transactions of the Royal Society-London 91, 123–137.

Steenken, A., Siegesmund, S., Heinrichs, T., 2000. The emplacement of the Riesenferner Pluton (Eastern Alps, Tyrol): constraints from field observations, magnetic fabrics and microstructures. Journal of Structural Geology 22, 1855–1873.

Tarling, D.H., Hrouda, F., 1993. The Magnetic Anisotropy of Rocks. Chapman and Hall, New York. 217pp.

Tomezzoli, R.N., MacDonald, W.D., Tickyj, H., 2003. Composite magnetic fabrics and S–C structure in granitic gneiss of Cerro de los Viejos, La Pampa province, Argentina. Journal of Structural Geology 25, 159–169.

Wada, Y., 1992. Magma flow directions inferred from preferred orientations of phenocryst in a composite feeder dike, Miyake-Jima, Japan. Journal of Volcanology and Geothermal Research 49, 119–126.

Wellington, S.L., Vinegar, H.J., 1987. X-ray computerized tomography. Journal of Petroleum Technology August 1987, 885–898.